JACS
JOURNAL OF THE AMERICAN CHEMICAL SOCIETY
Article
pubs.acs.org/JACS

Seed-Mediated Synthesis of Core/Shell FePtM/FePt (M = Pd, Au) Nanowires and Their Electrocatalysis for Oxygen Reduction Reaction

Shaojun Guo,[†] Sen Zhang,[†] Dong Su,[‡] and Shouheng Sun*,[†]

[†]Department of Chemistry, Brown University, Providence, Rhode Island 02912, United States
[‡]Center for Functional Nanomaterials, Brookhaven National Laboratory, Upton, New York 11973, United States

Supporting Information

ABSTRACT: We report a new seed-mediated growth of FePt over 2.5 nm wide FePtM (M = Pd, Au) nanowires (NWs) into core/shell FePtM/FePt NWs with controlled FePt shell thickness from 0.3 to 1.3 nm. These FePtM/FePt NWs show shell thickness and core composition-dependent electrocatalytic activity for oxygen reduction reaction (ORR) in 0.1 M $HClO_4$. These core/shell FePtM/FePt NWs are generally more active and durable than the corresponding alloy NWs. Among FePtM/FePt NWs, FePt NWs, FePtPd NWs, and commercial Pt studied, the FePtPd/FePt NWs (0.8 nm shell) show the specific activity of 3.47 mA·cm^{-2} and the mass activity of 1.68 A/mg Pt at 0.5 V (vs. Ag/AgCl), superior to all other NWs (less than 1.59 mA/cm^2 and 0.82 A/mg Pt for FePtAu/FePt and FePt) as well as the commercial Pt (0.24 mA/cm^2 and 0.141 A/mg Pt). The FePtM/FePt (0.8 nm shell) NWs are also stable in the ORR condition and show no activity decrease after 5000 potential sweeps between 0.4 and 0.8 V (vs Ag/AgCl). They are the most efficient nanocatalyst ever reported for ORR.

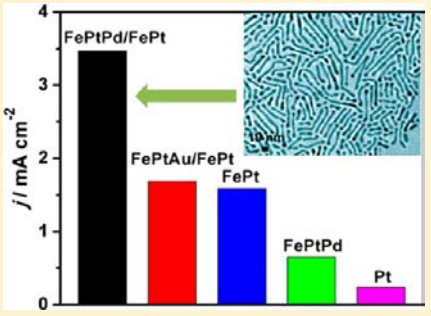

1. INTRODUCTION

The need to develop highly efficient electrochemical energy conversion devices, such as polymer electrolyte membrane fuel cells, requires effective electrocatalysts for both fuel oxidation reaction and oxygen reduction reaction (ORR).[1−5] Catalysts based on Pt nanoparticles (NPs) with different composition and geometric shapes have been explored extensively to enhance their catalysis for chemical conversion, especially for ORR.[1,6] Recently, core/shell NPs[7] and one-dimensional (1D) nanostructures[8−16] are found to be more promising in catalyzing ORR with much improved activity and durability. The core/shell structure with Pt present around the thin shell not only maximizes the Pt exposure to oxygen and minimizes the Pt use for catalysis, but also offers the desired core−shell interactions to tune both electronic and surface strain effects for optimal catalysis.[7] The catalytic efficiency increases even more when the 1D nanostructures serve as a catalyst,[11−16] as demonstrated more specifically in ∼2.5 nm wide MPt[13] and FePtM nanowires (NWs) for ORR catalysis.[14] It is believed that these NWs have much larger surface contact with the carbon support than the polyhedral NPs and therefore adhere to the carbon support more strongly, facilitating their stabilization and electron conduction during the catalysis. The promising data obtained from both core/shell and NW catalysts infer that the ORR catalysis would be further enhanced over a core/shell structured NW catalyst.

Here we report our studies on the synthesis of core/shell FePtM/FePt NWs and their enhanced catalysis for ORR. Recently core/shell FePt/FePt[13] and FePtCu/Pt[14] NWs were synthesized by either seed-mediated synthesis (FePt) or surface electrochemical dealloying (FePtCu/Pt). In these NW structures, early transition metals are readily etched, making it difficult to optimize the effect of M metals on Pt catalysis. An alternative NW catalyst system is to include Au or Pd in the 1D core structure because Au or Pd can further enhance Pt catalysis, as demonstrated in the core/shell Au/FePt[7b] and Pd/FePt[7a] NP catalysts. In this work, we prepared 2.5 nm wide FePtM NWs and found that these NWs could serve as seeds for FePt coating. We synthesized the core/shell FePtM/FePt NWs with FePt shell ranging from 0.3 to 1.3 nm and tested their ORR catalysis in 0.1 M $HClO_4$ solution. These NWs were indeed more active and durable than the seeding NWs. The optimal FePtPd/FePt NWs with 0.8 nm FePt shell had the specific activity of 3.47 mA/cm^2 and mass activity of 1.68 A·mg^{-1} at 0.5 V (vs. Ag/AgCl), much higher than what the commercial Pt had (0.24 mA/cm^2 and 0.141 A/mg Pt).

2. EXPERIMENTAL SECTION

2.1. Chemicals and Materials. Oleylamine (OAm, > 70%), 1-octadecene (ODE), sodium oleate, oleic acid (OA), $Pt(acac)_2$ (acac = aceylacetonate), $Pd(acac)_2$, $HAuCl_4·H_2O$, iron pentacarbonyl ($Fe(CO)_5$), hexane, isopropanol, ethanol, acetic acid (AA), and Nafion (5%) were all purchased from Sigma-Aldrich. The C−Pt catalyst (20% Pt mass loading containing 2.5−3.5 nm Pt NPs) was obtained from Fuel Cell Store.

2.2. NW Characterization. X-ray diffraction (XRD) patterns were collected on a Bruker AXS D8-Advanced diffractometer with Cu Kα radiation (λ =1.5418 Å). The inductively coupled plasma-atomic emission spectroscopy (ICP-AES) measurements were carried out on a JY2000 Ultrace ICP Atomic Emission spectrometer equipped with a

Received: June 17, 2013
Published: August 26, 2013

   dx.doi.org/10.1021/ja406091p | J. Am. Chem. Soc. 2013, 135, 13879−13884

JY AS 421 autosampler and 2400g/mm holographic grating. Transmission electron microscopy (TEM) images were acquired on a Philips CM 20 operating at 200 kV. Scanning transmission electron microscopy (STEM) analyses were carried out with a Hitachi HD2700C (200 kV) with a probe aberration-corrector in the Center for Functional Nanomaterials at Brookhaven National Lab. The 2D electron energy-loss spectroscopy (EELS) mapping was obtained by using a high-resolution Gatan-Enfina ER with a probe size of 1.3 Å. A power law function was used for EELS background subtraction. Samples for TEM and STEM analysis were prepared by depositing a single drop of diluted NWs dispersion in hexane on amorphous carbon coated copper grids.

2.3. Synthesis of FePtM (M = Au, Pd) and FePt NWs. FePtAu NWs were synthesized as follows. A 0.3-g sample of sodium oleate and 12 mL of ODE were mixed under magnetic stirring. Under a gentle flow of N_2, the mixture was heated to 200 °C to dissolve sodium oleate. Once the clear solution was formed, the heating temperature was lowered to 60 °C, and 0.2 g of $Pt(acac)_2$ and 8 mL of OAm were added. Under a N_2 blanket, the solution was heated to 110 °C and 0.09 mL of $Fe(CO)_5$ was injected. The solution was further heated to 190 °C at the heating rate of 4−5 deg/min so that a clear black solution was obtained. The solution was air-cooled to 120 °C within 5 min, and under a vigorous magnetic stirring, 68 mg of $HAuCl_4{\cdot}H_2O$ predissolved in a mixture of 1.2 mL of ODE and 0.8 mL of OAm was injected. The solution was heated to 240 °C at 4−5 deg/min and kept at this temperature for 30 min. The reaction mixture was cooled to 40−50 °C before 20 mL of hexane and 30 mL of ethanol were added to precipitate out the product, which was separated by centrifugation at 9000 rpm for 10 min and dispersed in hexane.

FePtPd NWs were prepared similarly except that 0.15 g of $Pt(acac)_2$, 0.115 g of $Pd(acac)_2$, and 0.07 mL of $Fe(CO)_5$ were used. This synthesis was different from what we published previously[17] and gave better seeding FePtPd NWs for the next-step seed-mediated growth.

FePt NWs were also synthesized similarly. After $Fe(CO)_5$ was injected, the mixture was heated directly to 240 °C at 4−5 deg/min and kept at this temperature for 30 min. The FePt NWs were used as a control.

2.4. Synthesis of FePtM/FePt Core/Shell NWs. A controlled amount of $Pt(acac)_2$ was dissolved in a mixture of 15 mL of ODE, 1.5 mL of OAm, and 1.5 mL of OA at 110 °C under a gentle flow of N_2. Thirty milligrams of FePtPd or FePtAu NWs dispersed in 2 mL of ODE was added and dissolved in the solution. Under a blanket of N_2, $Fe(CO)_5$ was added and the solution was heated to 200 °C at 4−5 deg/min and kept at this temperature for 20 min. The solution was cooled to room temperature, and 25 mL of ethanol was added, followed by centrifugation (8500 rpm, 8 min). The FePtM/FePt NWs were dispersed in 25 mL of hexane and reprecipitated by adding 25 mLof ethanol. The final product was dispersed in 10 mL of hexane for further use.

2.5. Preparation of C-NWs. A dispersion of 20 mg of NWs in 20 mL of hexane was added into 30 mL of hexane containing 40 mg of Ketjen carbon (EC-300J). The mixture was sonicated for 1 h. The solvent was decanted and the black solid powder was washed twice with ethanol. The powder was then suspended in 40 mL of AA and the suspension was heated at 70 °C for overnight to remove the surfactants around NWs.[18] The AA-treated C-NWs were separated by centrifugation, washed with water, and resuspended in a mixture containing water, isopropanol, and Nafion (5%) (v:v:v 4:1:0.025) to form a 2 mg/mL catalyst ink.

2.6. Eletrocatalysis for ORR. The electrochemical measurements were performed at room temperature on a potentiostat (Autolab 302). A glassy carbon (GC) rotating disk electrode (RDE) was used as the working electrode, and Ag/AgCl (4 M KCl) and Pt wire were used as the reference electrode and the counter electrode, respectively. Ten microliters of catalyst ink was cast on a newly polished GC-RDE and dried under ambient condition. Before data collection, all working electrodes were cleaned by a steady-state potential sweeping from −0.2 to 1.0 V at 50 mV/s in N_2-saturated 0.1 M $HClO_4$ solution. Once the current−potential curve was stable, the cyclic voltammogram (CV) at 50 mV/s was recorded. From this CV, the electrochemically active surface area (ECASA) of the NW catalyst was determined by integrating the area surrounded by the hydrogen desorption curve and the CV baseline. The scan rate and rotation rate for ORR measurement were 10 mV/s and 1600 rpm, respectively. The ORR kinetic currents were calculated from the Levich-Koutecky equation[19] and normalized to the amount of Pt and to ECASA to get mass and specific activities of the catalysts, respectively. The electrocatalytic results were obtained by averaging three independent measurements with an error margin <10%.

3. RESULTS AND DISCUSSION

The 2.5-nm wide FePtM (M = Pd, Au) NWs were first synthesized through thermal decomposition of $Fe(CO)_5$ and controlled consecutive reduction of $Pt(acac)_2$ and $Pd(acac)_2$ or $HAuCl_4$. The composition of FePtM was controlled by the molar ratio of M to $Pt(acac)_2$. Inductively coupled plasma-atomic emission spectroscopy (ICP-AES) was used to characterize the composition of the as-prepared FePtM NWs. In the above synthesis of FePtPd and FePtAu NWs, $Fe_{36}Pt_{32}Pd_{32}$ NWs and $Fe_{48}Pt_{37}Au_{15}$ were obtained. Figure S1A,B (Supporting Information) shows the typical transmission electron microscopy (TEM) images of $Fe_{36}Pt_{32}Pd_{32}$ (Figure S1A, SI) and $Fe_{48}Pt_{37}Au_{15}$ (Figure S1B, SI) NWs. These FePtM NWs have an average diameter about 2.5 nm and a typical length of 20−100 nm. The "nodes" along the wires are likely caused by the preferred growth at the tip of the wire in the OAm reverse micelle template.[20] Under the current condition, more Au- and Pd-rich FePtM NWs were difficult to obtain due to the separate nucleation and growth of elemental Au and Pd NPs at high Au and Pd salt concentrations.

By using these ultrathin $Fe_{36}Pt_{32}Pd_{32}$ and $Fe_{48}Pt_{37}Au_{15}$ NWs as seeds (30 mg), FePtM/FePt core/shell NWs with controlled shell thickness were easily made. For example, 0.02 mL of $Fe(CO)_5$ and 40 mg of $Pt(acac)_2$ gave FePtM/FePt NWs with a 0.3 nm shell, designated as FePtM/FePt-0.3 (Figure 1A,B), 0.04 mL of $Fe(CO)_5$ and 80 mg of $Pt(acac)_2$ resulted in a 0.8 nm FePt shell, designated as FePtM/FePt-0.8 (Figure 1C,D), and 0.06 mL of $Fe(CO)_5$ and 120 mg of $Pt(acac)_2$ yielded a 1.3 nm FePt shell, designated as FePtM/FePt-1.3 (Figure 1E,F). During the growth of the FePt shell with different thickness, the molar ratio of $Fe(CO)_5$ to $Pt(acac)_2$ was kept constant at 3:2. The final molar ratio of Fe to Pt on FePtPd/FePt and FePtAu/FePt NWs was around 22/78 and 26/74, respectively, which is lower than the seeding NWs, indicating the chemical etching of Fe upon Pt salt reduction.[17]

The structure of the core/shell NWs was further characterized by high-angle annular dark field (HAADF)-scanning transmission electron microscopy (STEM), STEM-electron energy-loss spectroscopy (STEM-EELS), and X-ray diffraction (XRD). Figure 2A shows the HAADF-STEM image of the FePtPd/FePt-0.8 NWs. Panels B and C of Figure 2 are the high-resolution (HR) HAADF-STEM images (Z-contrast) of a section of a single FePtPd-FePt NW. In Figure 2B, we observe a different lattice image at the shell and core areas. The shell thickness was directly measured to be ∼0.8 nm. Figure 2C is the middle section of the NW. The lattice fringes are clearly seen and the spacing of the adjacent fringes along the wire growth direction is 0.22 nm, corresponding to the {111} interplanar distance of face-centered cubic (*fcc*) FePt structure.[17] Elemental distribution of a representative FePtPd/FePt NW is investigated by 2D STEM-EELS mapping, as seen in Figure 2D,E. Along the NW, Pd (green) concentrates in the core region and Pt (blue) distributes evenly across the

dx.doi.org/10.1021/ja406091p | J. Am. Chem. Soc. 2013, 135, 13879−13884

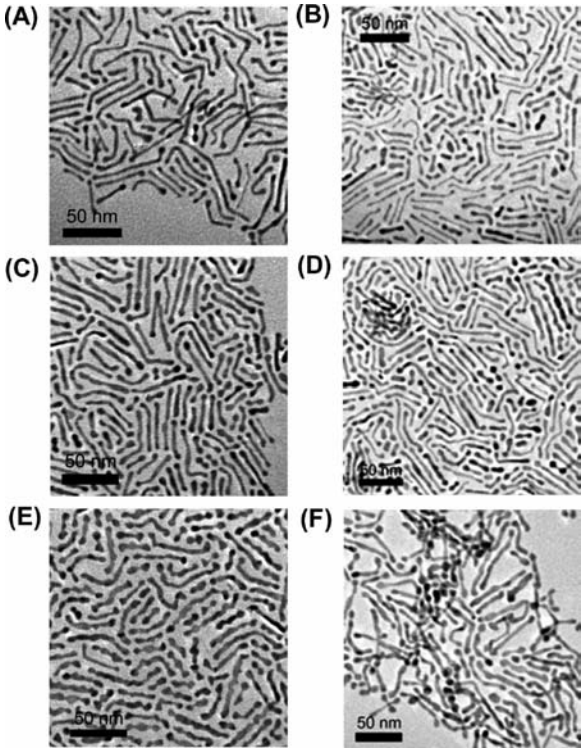

Figure 1. TEM images of FePtPd/FePt-0.3 (A), FePtAu/FePt-0.3 (B), FePtPd/FePt-0.8 (C), FePtAu/FePt-0.8 (D), FePtPd/FePt-1.3 (E), and FePtAu/FePt-1.3 (F).

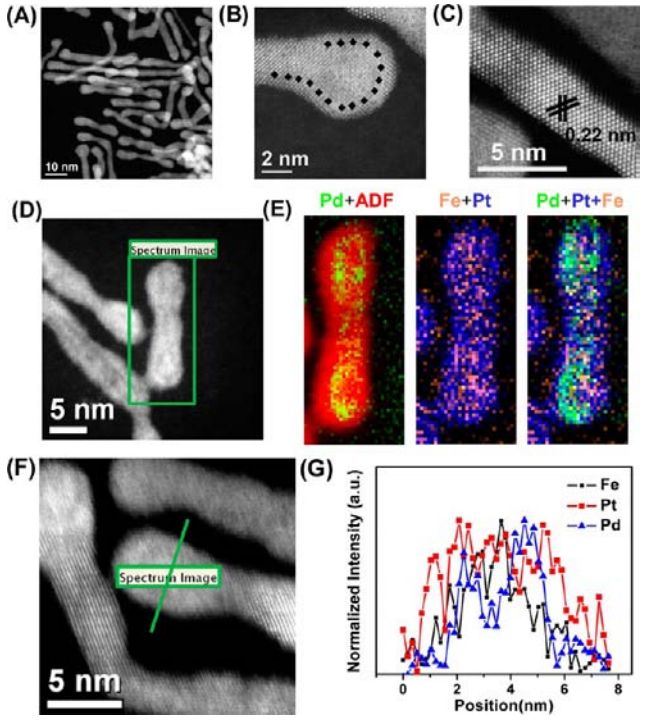

Figure 2. HAADF-STEM (A, D, F), high resolution HAADF-STEM (B, C), and STEM-EELS mapping (29 × 66 pixels, spatial resolution of 3 Å) (E) images of FePtPd/FePt-0.8. (F, G) High-resolution (1.7 Å) line-scan EELS analysis across one NW.

whole NW. More Fe (red) also locates inside the NW, indicating that the Pt-rich shell is indeed formed during the coating process. The core/shell structure was further confirmed by linear scan EELS with a higher spatial resolution across a single NW (Figure 2F,G). We can see that Pt is evenly distributed across the NW while Pd and Fe populate inside the NW.

Figures 3 and S2 (Supporting Information) show the XRD patterns of the FePt, FePtPd, FePtPd/FePt, as well as FePtAu

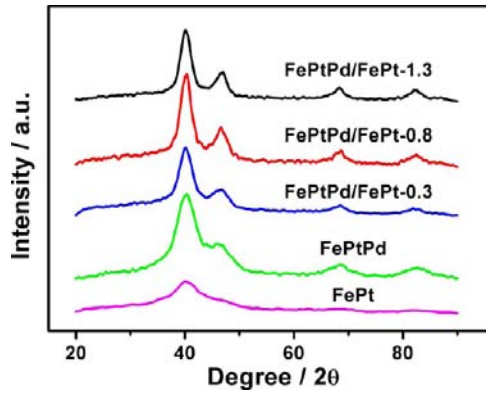

Figure 3. (A) XRD patterns of FePt, FePtPd, FePtPd/FePt-0.3, FePtPd/FePt-0.8, and FePtPd/FePt-1.3 NWs.

and FePtAu/FePt NWs. Their (111) peaks appear at the same diffraction angle due to the close lattice matching between Pd- (or Au) and Pt-based structures.[17] The (111) peak becomes narrower with thicker FePt coating, indicating that the crystal domains grow larger upon the FePt coating.

The ORR activity and stability of the FePtM/FePt NWs deposited on C (C-FePtM/FePt, Figure S3, Supporting Information) were studied in 0.1 M $HClO_4$ solution. Figure S4A (Supporting Information) shows the typical CVs of the C-FePtPd/FePt with different shell thickness in N_2-saturated 0.1 M $HClO_4$ at a sweep rate of 50 mV/s. Hydrogen adsorption/desorption appear in the range −0.2 to 0.15 V and metal oxidation/reduction occur in the range 0.4 to 0.9 V. The hydrogen desorption region was used to determine ECASA of the NWs. Figure 4A shows the ORR polarization curves of the C-FePtPd/FePt obtained at room temperature in O_2-saturated 0.1 M $HClO_4$ at 10 mV/s and a rotation speed of 1600 rpm. We can see that these C-FePtPd/FePt have similar ORR onset potential. But the C-FePtPd/FePt-0.8 exhibits a slightly more positive half-wave potential than the two other kinds of C-FePtPd/FePt. After being normalized over the NW ECASA, the FePtPd/FePt-0.8 NWs show the highest specific activity of 3.47 mA cm^{-2} in all FePtPd/FePt NWs investigated (Figure 4B). We further studied ORR stability of the FePtPd/FePt-0.8 NWs by scanning the potential between 0.4 and 0.8 V (vs Ag/AgCl) in the O_2-saturated 0.1 M $HClO_4$ at a scan rate of 100 mV/s. The CVs and ORR polarization curves of the FePtPd/FePt-0.8 NWs before and after 5000 potential cycles are shown in Figure 4C,D. After the stability test, the FePtPd/FePt-0.8 NWs only slightly lose their ECASA and have no ORR kinetic change. ICP-AES analysis on the C-FePtPd/FePt before and after the stability test showed nearly no Fe/Pt ratio changes (from 15/85 to 14/86). Furthermore, the morphology of the NWs was preserved after the stability test, as confirmed by the TEM images of the FePtPd/FePt-0.8 NWs before and after the stability test (Figure 4E,F).

The C-FePtAu/FePt NWs were also studied for ORR. Figures S4B (Supporting Information) and 5A show the CVs (Figure S4, Supporting Information) and ORR polarization

dx.doi.org/10.1021/ja406091p | J. Am. Chem. Soc. 2013, 135, 13879−13884

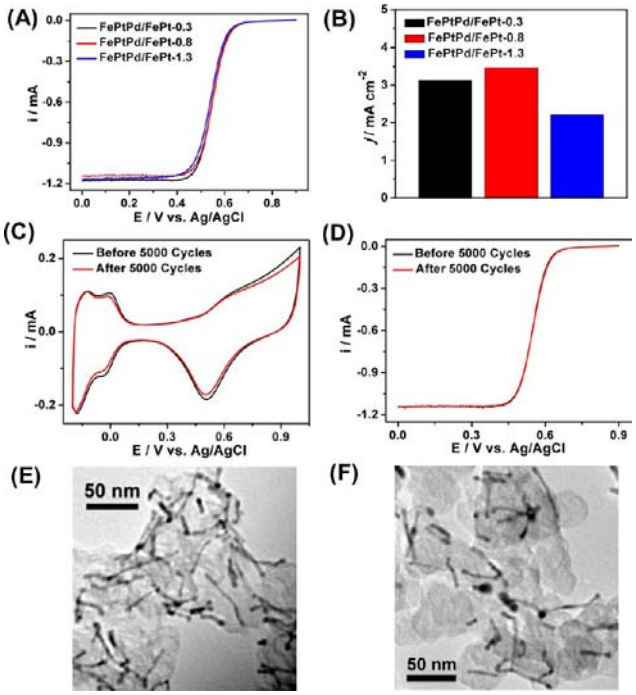

Figure 4. (A) ORR polarization curves of C-FePtPd/FePt-0.3, C-FePtPd/FePt-0.8, and C-FePtPd/FePt-1.3 in O_2-saturated 0.1 M $HClO_4$ solution at 293 K. (B) Summary of specific activities for ORR at 0.5 V vs Ag/AgCl (4 M KCl). (C) CVs and (D) polarization curves of the FePtPd/FePt-0.8 NWs before and after 5000 potential cycles between 0.4 and 0.8 V (vs Ag/AgCl). (E, F) TEM images of the C-FePtPd/FePt-0.8 NWs before (E) and after (F) stability test.

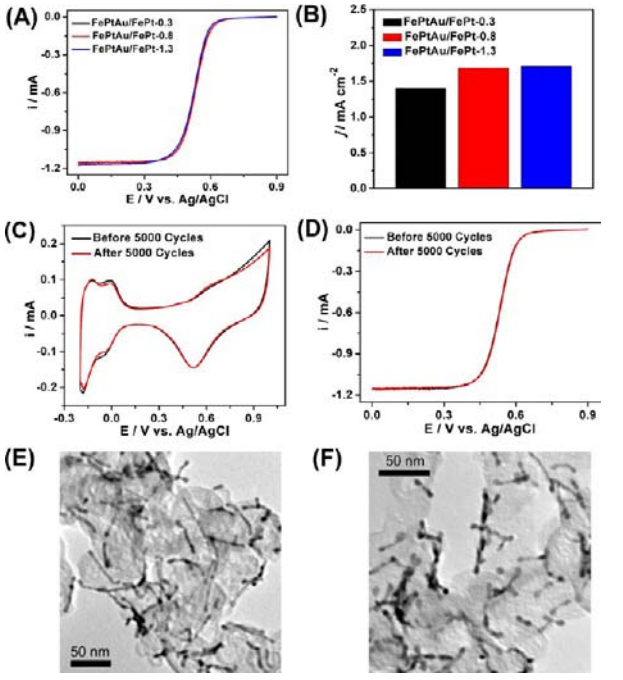

Figure 5. (A) ORR polarization curves of C-FePtAu/FePt-0.3, C-FePtAu/FePt-0.8, and C-FePtAu/FePt-1.3. (B) Summary of specific activities for ORR at 0.5 V vs Ag/AgCl (4 M KCl). (C) CVs and (D) ORR polarization curves of C-FePtAu/FePt-0.8 NWs before and after 5000 potential cycles between 0.4 and 0.8 V (vs Ag/AgCl). (E, F) TEM images of the C-FePtAu/FePt-2 NWs before (E) and after (F) stability test.

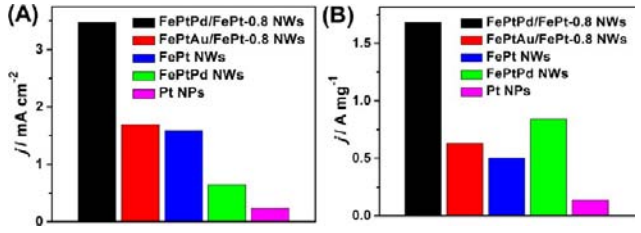

Figure 6. ORR specific (A) and mass (B) activity summaries of the FePtPd/FePt-0.8, FePtAu/FePt-0.8, FePt, and FePtPd NWs as well as the commercial Pt NPs at 0.5 V vs Ag/AgCl (4 M KCl).

curves (Figure 5A) for the C-FePtAu/FePt NWs. All three different C-FePtAu/FePt have nearly the same ORR polarization curves and similar specific ORR activity (Figure 5B). It seems that different from Pd in the FePtPd/FePt structure, Au in the core has little effect on ORR activity of the FePt shell. Nevertheless, C-FePtAu/FePt does show the desired stability, as demonstrated by the C-FePtAu/FePt-0.8 in their CVs (Figure 5C), ORR polarization curves (Figure 5D), and TEM images (Figure 5E,F).

Electrocatalytic activities of different NW catalysts were further normalized and compared with the commercial Pt catalyst. Figure S5A,B (Supporting Information) shows the CVs (A) and ORR polarization curves (B), and Figure 6 summarizes the specific (A) and mass activities (B) comparisons (j_k, kinetic current density) of the FePtPd/FePt-0.8, FePtAu/FePt-0.8, FePt, and FePtPd NWs as well as commercial Pt catalysts at 0.5 V. Among these catalysts, the FePtPd-FePt-0.8 NWs show the highest specific activity, reaching 3.47 mA/cm^2, much higher than the FePtAu-FePt-0.8 NWs (1.69 mA/cm^2), FePt NWs (1.59 mA/cm^2), FePtPd NWs (0.65 mA/cm^2), and commercial Pt (0.24 mA/cm^2). We can conclude that compared to Au, Pd in the core/shell NWs does help to enhance ORR activity to a greater degree. The Pt mass activity of the FePtPd-FePt-0.8 NWs is 1.68 A/mg Pt. As a comparison, the mass activity of the commercial Pt is at 0.141 A/mg Pt.

Recent studies in multicomponent NP catalyst for ORR have revealed that Au is more electropositive than Pt and can efficiently stabilize Pt from easy oxidation during ORR.[21] Using Au as a stabilizer, core/shell structured Au/FePt NPs have been synthesized and studied for ORR. Indeed Au/FePt NPs are much more stable than the Pt or FePt NP catalysts in ORR conditions.[7b] Furthermore, Fe in the FePt shell does help to improve ORR activity due to the alloy effect,[22] making the Au/FePt more active and stable than Pt for ORR. Compared with Au, Pd is less electropositive and coupling Pd to Pt cannot improve catalyst stability unless Pd/FePt core/shell structure is made.[7a] On shape-dependent catalytic studies, ultrathin NWs, such as FePt and CoPt NWs,[13] are found to be more efficient catalysts for ORR due to their stronger adsorption to carbon microparticles and their better electron conductivity between the reaction sites and the carbon support. But adding Pd to FePt NWs, as seen in trimetallic FePtPd alloy NWs, does not improve the ORR catalysis of these NWs, rather it makes them better catalysts for the methanol oxidation reaction.[17] Combining what we have learned from the core/shell and NW structures, we can conclude that the Au and Pd effect on ORR is better demonstrated in a core/shell NW structure. We have tested the synthesis of Au and Pd NWs for FePt coating but failed. However, FePtPd and FePtAu NWs are readily prepared to serve as seeds. Therefore, we have synthesized

dx.doi.org/10.1021/ja406091p | J. Am. Chem. Soc. 2013, 135, 13879−13884

FePtM/FePt NWs with FePt shell thickness controlled in less than 1.5 nm. Such FePtM/FePt provides an excellent NW platform for studying the M effect on ORR. Indeed, with FePtPd/FePt NWs, we have a new class of core/shell electrocatalysts that are even more efficient than FePt NWs for ORR. From Figure 6, we can see that the specific and mass activities of the FePtPd/FePt NWs are about 2.2 and 3.4 times those from the FePt NWs. Different from Pd, Au does not improve the ORR activity in the FePtAu/FePt NW structure—the slight activity increase shown in Figure 6 is from the Fe alloy effect,[22] but it does stabilize the core/shell NW catalyst in the ORR condition. The higher ORR activity observed from the FePtPd/FePt NWs than from the FePtAu/FePt NWs may be attributed to the electronic effect of Pd to FePt, which further downshifts the *d*-band center of Pt, facilitating O_2 adsorption, activation, and desorption.[7a,22] In the ORR stability tests, both FePtAu/FePt and FePtPd/FePt core/shell NWs show impressive stability without activity degradation after 5000 potential cycling between 0.4 and 0.8 V (vs. Ag/AgCl). This stability enhancement comes likely from both strong NW/carbon support interaction and the controlled Pt−Pt strain in the core/shell structure. We should mention that in the FePtM/FePt structure, too thin a coating cannot form a uniform shell around the core and too thick a coating makes the NWs similar to pure FePt NWs. A 0.8 nm coating seems to be critical to form uniform coating and for the shell to "feel" the core effect on its *d*-band shift (electronic effect) and Pt−Pt distance (strain effect). All in all, the FePtPd/FePt NWs with a 0.8 nm FePt shell are the most efficient NW catalysts ever reported for ORR.

4. CONCLUSIONS

We have developed a seed-mediated growth method to prepare core/shell FePtM/FePt (M = Pd, Au) NWs. Through controlled decomposition of $Fe(CO)_5$ and reduction of $Pt(acac)_2$ in the presence of 2.5 nm wide FePtM NW seeds, 0.3−1.3 nm thick FePt shell can be deposited around the FePtM core. These FePtM/FePt NWs have shell thickness and core composition-dependent activity for ORR in 0.1 M $HClO_4$ solution and the FePtPd/FePt-0.8 NWs have the highest activity: their specific and mass activities reach 3.47 mA/cm^2 and 1.68 A/mg at 0.5 V (vs. Ag/AgCl), respectively, which are 2.2 and 3.4 times higher than those of FePt NWs, and 14.5 and 12.5 times higher than the values from the commercial Pt catalyst. The present FePtM/FePt-0.8 NWs are also stable in the ORR condition and have nearly no ECASA drop, no ORR polarization curve shift, and no NW morphology change after 5000 potential cycling between 0.4 and 0.8 V (vs. Ag/AgCl). The core/shell FePtM/FePt NWs, especially the FePtPd/FePt-0.8 NWs, are the most efficient NW catalyst ever reported for ORR. The synthetic concept demonstrated here is not limited to FePtM/FePt, but can be extended to other multimetallic core/shell NWs containing Ni and Co. These core/shell NWs should be robust and have high potentials to serve as commercially viable catalysts for ORR and for fuel cell applications.

■ ASSOCIATED CONTENT

Supporting Information

Figures S1 to S5 giving TEM images, XRD patterns and CVs. This material is available free of charge via the Internet at http://pubs.acs.org.

■ AUTHOR INFORMATION

Corresponding Author

ssun@brown.edu

Author Contributions

Shaojun Guo and Sen Zhang contributed equally to this work.

Notes

The authors declare no competing financial interest.

■ ACKNOWLEDGMENTS

This work was upported by the U.S. Army Research Laboratory and the U.S. Army Research Office under the Multi University Research Initiative (MURI, grant number W911NF-11-1-0353) on "Stress-Controlled Catalysis via Engineered Nanostructures", and by the U.S. Department of Energy, Office of Energy Efficiency and Renewable Energy, Fuel Cell Technologies Program. Electron microscopy work carried out at the Center for Functional Nanomaterials, Brookhaven National Laboratory, was supported by the U.S. Department of Energy, Office of Basic Energy Sciences, under Contract No. DE-AC02-98CH10886.

■ REFERENCES

(1) (a) Wu, J.; Gross, A.; Yang, H. *Nano Lett.* **2011**, *11*, 798−802. (b) Zhang, J.; Fang, J. *J. Am. Chem. Soc.* **2009**, *131*, 18543−18547. (c) Zhang, J.; Yang, H.; Fang, J.; Zou, S. *Nano Lett.* **2010**, *10*, 638−644. (d) Xu, D.; Bliznakov, S.; Liu, Z.; Fang, J.; Dimitrov, N. *Angew. Chem., Int. Ed.* **2010**, *49*, 1282−1285. (e) Xu, D.; Liu, Z.; Yang, H.; Liu, Q.; Zhang, J.; Fang, J.; Zou, S.; Sun, K. *Angew. Chem., Int. Ed.* **2009**, *48*, 4217−4221. (f) Yang, H.; Zhang, J.; Sun, K.; Zou, S.; Fang, J. *Angew. Chem., Int. Ed.* **2010**, *49*, 6848−6851. (g) Guo, S.; Sun, S. *J. Am. Chem. Soc.* **2012**, *134*, 2492−2495. (h) Wu, J.; Qi, L.; You, H.; Gross, A.; Li, J.; Yang, H. *J. Am. Chem. Soc.* **2012**, *134*, 11880−11883. (i) Zhou, W.; Wu, J.; Yang, H. *Nano Lett.* **2013**, *13*, 2870−2874. (j) Liang, Y.; Li, Y.; Wang, H.; Zhou, J.; Wang, J.; Regier, T.; Dai, H. *Nat. Mater.* **2011**, *10*, 780−786. (k) Guo, S.; Zhang, S.; Wu, L.; Sun, S. *Angew. Chem., Int. Ed.* **2012**, *51*, 11770−11773. (l) Li, Y.; Zhou, W.; Wang, H.; Xie, L.; Liang, Y.; Wei, F.; Idrobo, J.-C.; Pennycook, S. J.; Dai, H. *Nat. Nanotechnol.* **2012**, *7*, 394−400. (m) Kim, J.; Lee, Y.; Sun, S. *J. Am. Chem. Soc.* **2010**, *132*, 4996−4997. (n) Chou, S.-W.; Shyue, J.-J.; Chien, C.-H.; Chen, C.-C.; Chen, Y.-Y.; Chou, P.-T. *Chem. Mater.* **2012**, *24*, 2527−2533. (o) Wanjala, B. N.; Fang, B.; Luo, J.; Chen, Y.; Yin, J.; Engelhard, M. H.; Loukrakpam, R.; Zhong, C.-J. *J. Am. Chem. Soc.* **2011**, *133*, 12714−12727.

(2) (a) Wang, S.; Yu, D.; Dai, L. *J. Am. Chem. Soc.* **2011**, *133*, 5182−5185. (b) Wang, S.; Yu, D.; Dai, L.; Chang, D. W.; Baek, J.-B. *ACS Nano* **2011**, *5*, 6202−6209. (c) Wang, S.; Iyyamperumal, E.; Roy, A.; Xue, Y.; Yu, D.; Dai, L. *Angew. Chem., Int. Ed.* **2011**, *50*, 11756−11760. (d) Gong, K.; Du, F.; Xia, Z.; Durstock, M.; Dai, L. *Science* **2009**, *323*, 760−764. (e) Suntivich, J.; Gasteiger, H. A.; Yabuuchi, N.; Nakanishi, H.; Goodenough, J. B.; Yang, S.-H. *Nat. Chem.* **2011**, *3*, 546−550.

(3) (a) Guo, S.; Wang, E. *Nano Today* **2011**, *6*, 240−264. (b) Guo, S. J.; Dong, S. J. *Chem. Soc. Rev.* **2011**, *40*, 2644−2672. (c) Guo, S.; Wang, E. *Acc. Chem. Res.* **2011**, *44*, 491−500.

(4) (a) Bing, Y.; Liu, H.; Zhang, L.; Ghosh, D.; Zhang, J. *Chem. Soc. Rev.* **2010**, *39*, 2184−2202. (b) Mazumder, V.; Lee, Y.; Sun, S. *Adv. Funct. Mater.* **2010**, *20*, 1224−1231. (c) Liu, Y.; Li, D.; Sun, S. *J. Mater. Chem.* **2011**, *21*, 12579−12587.

(5) Wang, Y.-J.; Wilkinson, D. P.; Zhang, J. *Chem. Rev.* **2011**, *111*, 7625−7651.

(6) Guo, S.; Zhang, S.; Sun, S. *Angew. Chem., Int. Ed.* **2013**, *125*, 8686−8705.

(7) See e.g.: (a) Mazumder, V.; Chi, M.; More, K. L.; Sun, S. *J. Am. Chem. Soc.* **2010**, *132*, 7848−7849. (b) Wang, C.; van der Vliet, D.; More, K. L.; Zaluzec, N. J.; Peng, S.; Sun, S.; Daimon, H.; Wang, G.; Greeley, J.; Pearson, J.; Paulikas, A. P.; Karapetrov, G.; Strmcnik, D.; Markovic, N. M.; Stamenkovic, V. R. *Nano Lett.* **2011**, *11*, 919−926.

(c) Mazumder, V.; Chi, M.; More, K. L.; Sun, S. *Angew. Chem., Int. Ed.* **2010**, *49*, 9368−9372. (d) Wang, J. X.; Inada, H.; Wu, L.; Zhu, Y.; Choi, Y.; Liu, P.; Zhou, W.-P.; Adzic, R. R. *J. Am. Chem. Soc.* **2009**, *131*, 17298−17302. (e) Ghosh, T.; Vukmirovic, M. B.; DiSalvo, F. J.; Adzic, R. R. *J. Am. Chem. Soc.* **2010**, *132*, 906−907. (f) Gong, K.; Su, D.; Adzic, R. R. *J. Am. Chem. Soc.* **2010**, *132*, 14364−14366. (g) Wang, C.; Chi, M.; Li, D.; Strmcnik, D.; van der Vliet, D.; Wang, G.; Komanicky, V.; Chang, K.-C.; Paulikas, A. P.; Tripkovic, D.; Pearson, J.; More, K. L.; Markovic, N. M.; Stamenkovic, V. R. *J. Am. Chem. Soc.* **2011**, *133*, 14396−14403. (h) Gan, L.; Heggen, M.; Rudi, S.; Strasser, P. *Nano Lett.* **2012**, *12*, 5423−5430.

(8) Sun, S.; Zhang, G.; Geng, D.; Chen, Y.; Li, R.; Cai, M.; Sun, X. *Angew. Chem., Int. Ed.* **2011**, *50*, 422−426.

(9) Xia, B. Y.; Ng, W. T.; Wu, H. B.; Wang, X.; Lou, X. W. *Angew. Chem., Int. Ed.* **2012**, *51*, 7213−7216.

(10) Chen, Z.; Waje, M.; Li, W.; Yan, Y. *Angew. Chem., Int. Ed.* **2007**, *46*, 4060−4063.

(11) (a) Liang, H.-W.; Cao, X.; Zhou, F.; Cui, C.-H.; Zhang, W.-J.; Yu, S.-H. *Adv. Mater.* **2011**, *23*, 1467−1471. (b) Cui, C.-H.; Li, H.-H.; Yu, J.-W.; Gao, M.-R.; Yu, S.-H. *Angew. Chem., Int. Ed.* **2010**, *49*, 9149−9152. (c) Cui, C.-H.; Yu, S.-H. *Acc. Chem. Res.* **2013**, *46*, 1427−1437.

(12) Koenigsmann, C.; Zhou, W.-P.; Adzic, R. R.; Sutter, E.; Wong, S. S. *Nano Lett.* **2010**, *10*, 2806−2811.

(13) Guo, S.; Li, D.; Zhu, H.; Zhang, S.; Stamenkovic, V. R.; Sun, S. *Angew. Chem., Int. Ed.* **2013**, *52*, 3465−3468.

(14) Zhu, H.; Zhang, S.; Guo, S.; Su, D.; Sun, S. *J. Am. Chem. Soc.* **2013**, *135*, 7130−7133.

(15) Koenigsmann, C.; Santulli, A. C.; Gong, K.; Vukmirovic, M. B.; Zhou, W.-P.; Sutter, E.; Wong, S. S.; Adzic, R. R. *J. Am. Chem. Soc.* **2011**, *133*, 9783−9795.

(16) Koenigsmann, C.; Sutter, E.; Adzic, R. R.; Wong, S. S. *J. Phys. Chem. C* **2012**, *116*, 15297−15306.

(17) Guo, S.; Zhang, S.; Sun, X.; Sun, S. *J. Am. Chem. Soc.* **2011**, *133*, 15354−15357.

(18) Mazumder, V.; Sun, S. *J. Am. Chem. Soc.* **2009**, *131*, 4588−4589.

(19) (a) Lim, B.; Jiang, M.; Camargo, P. H. C.; Cho, E. C.; Tao, J.; Lu, X.; Zhu, Y.; Xia, Y. *Science* **2009**, *324*, 1302−1305. (b) Zhang, H.; Jin, M.; Wang, J.; Li, W.; Camargo, P. H. C.; Kim, M. J.; Yang, D.; Xie, Z.; Xia, Y. *J. Am. Chem. Soc.* **2011**, *133*, 6078−6089. (c) Lim, B.; Wang, J.; Camargo, P. H. C.; Jiang, M.; Kim, M. J.; Xia, Y. *Nano Lett.* **2008**, *8*, 2535−2540.

(20) Wang, C.; Hou, Y.; Kim, J.; Sun, S. *Angew. Chem., Int. Ed.* **2007**, *46*, 6333−6335.

(21) Zhang, J.; Sasaki, K.; Sutter, E.; Adzic, R. R. *Science* **2007**, *315*, 220−222.

(22) (a) Stamenkovic, V. R.; Mun, B.; Arenz, S. M.; Mayrhofer, K. J.; Lucas, C. A.; Wang, G.; Ross, P. N.; Markovic, N. M. *Nat. Mater.* **2007**, *6*, 241−247. (b) Stamenkovic, V. R.; Fowler, B.; Mun, B. S.; Wang, G. F.; Ross, P. N.; Lucas, C. A.; Markovic, N. M. *Science* **2007**, *315*, 493−497.